ACS OMEGA

Article

Cite This: ACS Omega 2019, 4, 16916−16924

http://pubs.acs.org/journal/acsodf

Ultrahigh Selective Room-Temperature Ammonia Gas Sensor Based on Tin−Titanium Dioxide/reduced Graphene/Carbon Nanotube Nanocomposites by the Solvothermal Method

Yotsarayuth Seekaew, Weeraphat Pon-On, and Chatchawal Wongchoosuk*

Department of Physics, Faculty of Science, Kasetsart University, Chatuchak, Bangkok 10900, Thailand

Supporting Information

ABSTRACT: Resistive-based gas sensors have been considered as the most favorable gas sensors for detection of toxic gases and volatile organic compounds (VOCs) because of their simple structure, low cost, high sensitivity, ease of use, and high stability. Unfortunately, wide application of resistive-based gas sensors is limited by their low selectivity. In this article, we present the fabrication of ultrahigh selective NH_3 gas sensor based on tin−titanium dioxide/reduced graphene/carbon nanotube (Sn−TiO_2@rGO/CNT) nanocomposites. The Sn−TiO_2@rGO/CNT nanocomposites with different molar ratios of Sn/Ti (1:10, 3:10, and 5:10) were synthesized via the solvothermal method. Characterizations by scanning electron microscopy, transmission electron microscopy, and X-ray photoelectron spectroscopy confirmed the decoration of Sn−TiO_2 nanoparticles on rGO/CNT nanocomposite surfaces. The Sn−TiO_2@rGO/CNT nanocomposite gas sensor exhibited high response and ultrahigh selectivity to NH_3 against toluene, dimethylformamide, acetone, ethanol, methanol, isopropanol, formaldehyde, hydrogen, carbon dioxide, acetylene, and VOCs in paint thinners at room temperature. The Sn−TiO_2@rGO/CNT nanocomposite gas sensor with molar ratio of Sn/Ti = 1:10 showed the highest response to NH_3 over other molar ratios of Sn/Ti as well as pure rGO/CNT and Sn−TiO_2 gas sensors. The ammonia-sensing mechanisms of the Sn−TiO_2@rGO/CNT gas sensor were proposed based on the formation of p−n heterojunctions of p-type rGO/CNT and n-type Sn−TiO_2 nanoparticles via a low-temperature oxidizing reaction process.

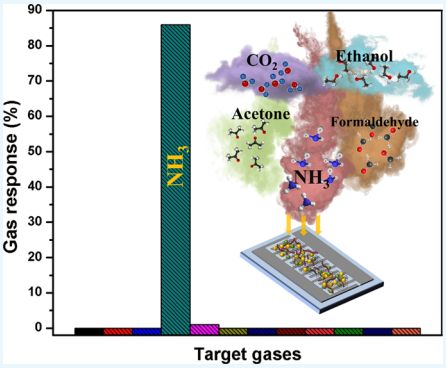

1. INTRODUCTION

Ammonia (NH_3) is one of the toxic gases that can cause illness or death when it is inhaled or absorbed by eyes, nose, skin, and the respiratory tract at high concentration.[1] NH_3 has been widely used in several commercial products and industrial applications such as ice factory, adhesives, rubber cements, automotive fuels, and laboratory solvents.[2−4] Moreover, NH_3 is also found in the exhaled breath of humans, in which it plays an important biomarker for diagnosis of kidney disorders or ulcers caused by the *Helicobacter pylori* bacterial stomach infection.[5,6] The exhaled breath of patients with kidney disorders and peptic ulcer releases NH_3 in the concentration range of 0.82−14.7 ppm.[7] Furthermore, NH_3 is produced from farming areas or animal agriculture that can affect health of humans, animals, and environment.[8] Therefore, detection of NH_3 is necessary for life saving, environment protection, and medical applications. Nowadays, sensing nanomaterials and fabrication techniques for NH_3 gas sensors have been extensively studied in term of high sensitivity, high selectivity, high stability, fast response, low cost, and ease of use. Metal oxides are one of the most popular NH_3-sensing nanomaterials. However, most NH_3 gas sensors based on metal oxides require high working temperatures of 150−300 °C and exhibit cross-sensitivity.[9,10] The development of room-temperature NH_3 gas sensors based on nanocomposites[11−14] is a way to overcome these crucial problems but until now no nanocomposites exhibited perfect selectivity to NH_3, leading to impractical use in real-world applications based on single gas detection with quantitative purpose.

A nanocomposite is defined as a multicomponent material in which at least one of components are of nanoscale size. It generally comprises multiphase inorganic/organic materials such as metal−metal oxides ($Ni_{60}Fe_{30}Mn_{10}$, Sn/Cu/ZnO NPs, MoS_2−Au, MoS_2/ZnO, and Cu−BTC/BNNT),[15−19] metal oxide−carbon nanomaterials (TiO_2−RGO, $CoFe_2O_4$/graphene, and rGO/MoS_2),[20−22] metal oxide−polymer (Pd−TiO_2@PPy, PANI/SnO_2, and PPy/Fe_2O_3),[23,24] and metal oxide−carbon nanomaterials−polymer (Pd−PANI−rGO, TiO_2@PPy−GN, graphene−PEDOT:PSS, and Pt/PAN−MWCNTs/WGE).[25−28] Among them, the hybrid carbon-based nanostructures have become one of the most attractive materials that can provide multidisciplinary applications, including flexible battery, biosensor, solar cell, super-capacitors, chemical sensor, and gas sensing,[29−31] due to their unique properties such as low-cost production, strong covalent-bond structures, large specific surface area, high electrical con-

Received: July 15, 2019
Accepted: September 23, 2019
Published: October 3, 2019

DOI: 10.1021/acsomega.9b02185
ACS Omega 2019, 4, 16916−16924

ductivity, low redox potential, and high mechanical strength.[32−34] In this work, we focus on new metal oxide−carbon nanocomposites consisting of tin−titanium dioxide/reduced graphene/carbon nanotube (Sn−TiO_2@rGO/CNT) for NH_3-sensing application at room temperature. The Sn−TiO_2@rGO/CNT nanocomposites were synthesized by the solvothermal process and characterized via scanning electron microscopy (SEM), transmission electron microscopy (TEM), and X-ray photoelectron spectroscopy (XPS). The sensing performances of Sn−TiO_2@rGO/CNT nanocomposites were systematically investigated. The NH_3-sensing mechanism was proposed based on the formation of p−n heterojunctions.

2. RESULTS AND DISCUSSION

2.1. Characterization of Sensing Films. The SEM image of Sn−TiO_2@rGO/CNT nanocomposite is shown in Figure 1a. It illustrates agglomeration of rGO and CNT leading to

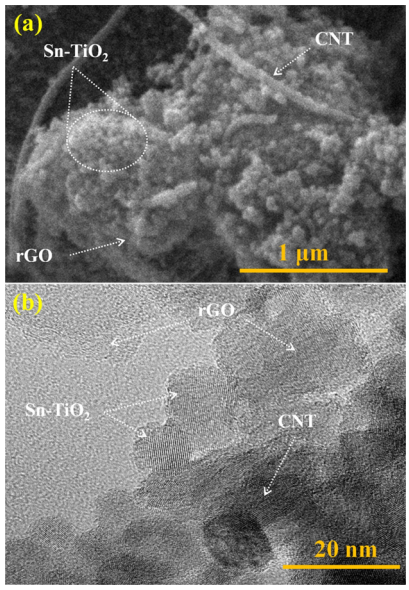

Figure 1. (a) SEM and (b) TEM images of Sn−TiO_2@rGO/CNT nanocomposite.

self-assembled 3D hierarchical interconnected morphology, whereas the Sn−TiO_2 nanoparticles are randomly embedded on the surface of the rGO/CNT nanocomposite. The corresponding TEM image confirms the coexistence of Sn−TiO_2 nanoparticles, graphene, and CNTs as demonstrated in Figure 1b. It can be seen that the Sn−TiO_2 nanoparticles with diameters of <15 nm are widely coated on graphene and CNT surfaces.

XPS survey scan measurements were performed to investigate the chemical composition of the Sn−TiO_2@rGO/CNT nanocomposite as illustrated in Figure 2. The survey scan XPS spectra of Sn−TiO_2@rGO/CNT with different molar ratios of Sn/Ti confirm the presence of C, Ti, Sn, and O in agreement with the expected chemical compositions of the Sn−TiO_2@rGO/CNT nanocomposite. The Sn atomic contents of Sn−TiO_2@rGO/CNT nanocomposites were calculated from the XPS data to be around 2.9, 3.8, and 5.4 at. % for nanocomposite I, nanocomposite II, and nanocomposite III, respectively. It can be seen that the Sn adding amounts increase approximately linearly with increasing Sn in TiO_2@rGO/CNT based on solvothermal method. In addition, all

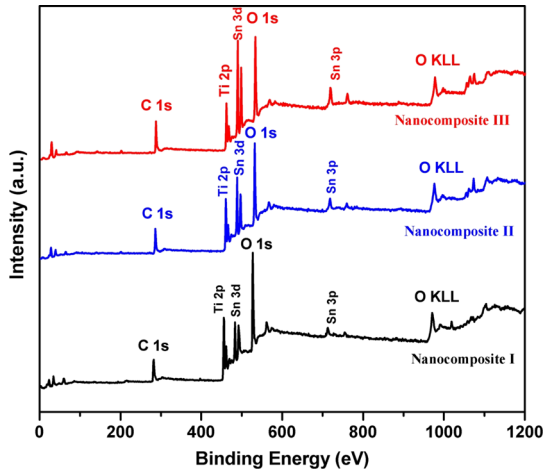

Figure 2. XPS survey scan spectra of Sn−TiO_2@rGO/CNT nanocomposite.

element atomic contents of nanocomposite I were found to be around C 1s (40.7 at. %), Ti (12.6 at. %), Sn (2.9 at. %), and O 1s (43.8 at. %).

The high-resolution C 1s peak (Figure 3a) can be deconvoluted into five peaks located at 283.3, 284.8, 286.1, 286.9 and 288.6 eV which correspond to C═C, C−C, C−OH, C−O, and COOH groups in rGO/CNT, respectively.[35−40] The C═C and C−C components refer to the backbone of the rGO/CNT structure, whereas the C−OH, C−O, and COOH bonds indicate the oxygen-containing functional groups. It can be seen that the C═C and C−C bonds have higher intensity than the oxygen-containing functional groups of C−OH, C−O, and COOH bonds. XPS spectra of Sn 3d and Ti 2p in nanocomposite I are presented in Figure 3b,c, respectively. Two peaks of Sn 3d spectrum at 486.6 and 495.0 eV are attributable to Sn $3d_{5/2}$ and Sn $3d_{3/2}$ spin orbit peaks of the Sn^{4+} state in SnO_2, confirming the formation of SnO_2 nanoparticles in the Sn−TiO_2@rGO/CNT nanocomposite.[41,42] For Ti 2p spectrum, two spin−orbit peaks of Ti $2p_{3/2}$ and Ti $2p_{1/2}$ are located at 458.8 and 464.5 eV, respectively. The two prominent peaks can be assigned to the Ti^{4+} state of TiO_2.[41,43] The high-resolution O 1s XPS spectrum of the nanocomposite I is shown in Figure 3d, the O 1s peak can be decomposed into four contributions centered at 529.9, 531.1, 531.9 and 532.9 eV, which can be attributed to O−metal (Sn, Ti) bonding,[44−46] Sn−O−C or Ti−O−C,[47,48] Sn−OH or Ti−OH,[49] and C−OH/C−O−C,[50] respectively.

2.2. Gas Sensing Properties. Figure 4a shows the change in resistance of the nanocomposite I gas sensor upon exposure to NH_3 vapor with different concentrations ranging from 25 to 250 ppm at room temperature. It is seen that the Sn−TiO_2@rGO/CNT gas sensor exhibits a rapid decrease of resistance upon exposure to NH_3 vapor before recovering to their baseline values in dry air. The resistance changing behaviors may be attributed to the adsorption and desorption of NH_3 molecules of the sensing films. The details of sensing mechanism for the Sn−TiO_2@rGO/CNT gas sensor will be discussed in the next section. The nanocomposite I gas sensor has been further tested to evaluate reproducibility under exposure to 250 ppm NH_3 vapor at room temperature as demonstrated in Figure 4b. It demonstrates that the Sn−TiO_2@rGO/CNT gas sensor can fully recover to their initial baselines for several repeated cycles. Consequently, the Sn−

DOI: 10.1021/acsomega.9b02185
ACS Omega 2019, 4, 16916−16924

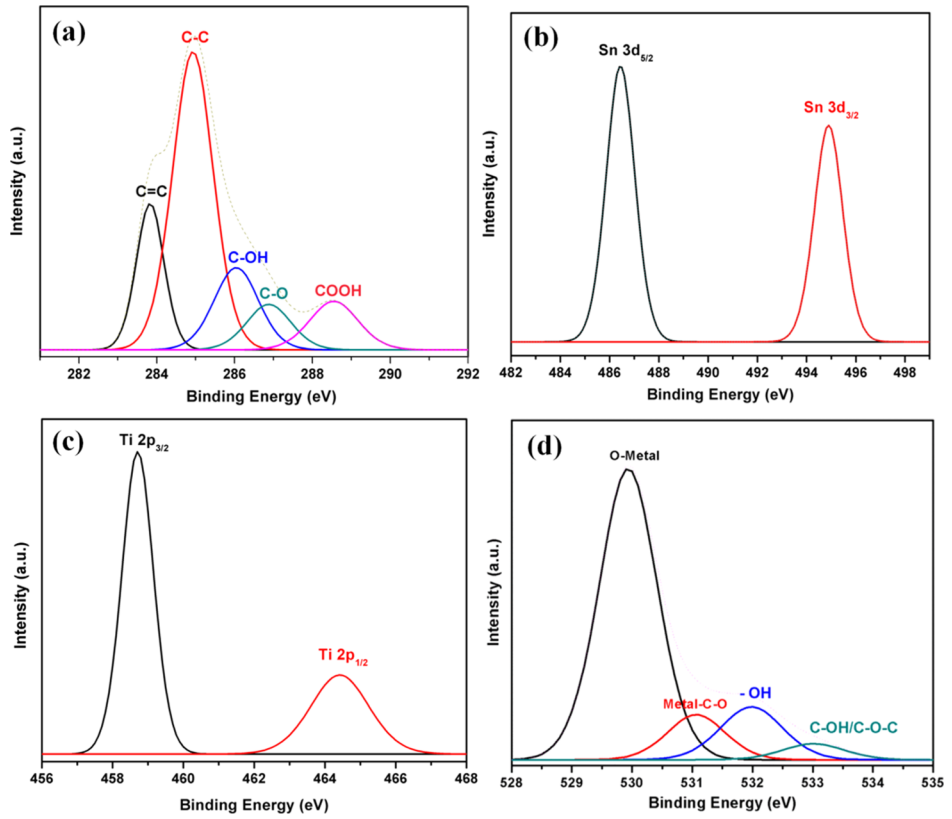

Figure 3. The high-resolution XPS spectra of the nanocomposite I for (a) C 1s, (b) Sn 3d, (c) Ti 2p, and (d) O 1s.

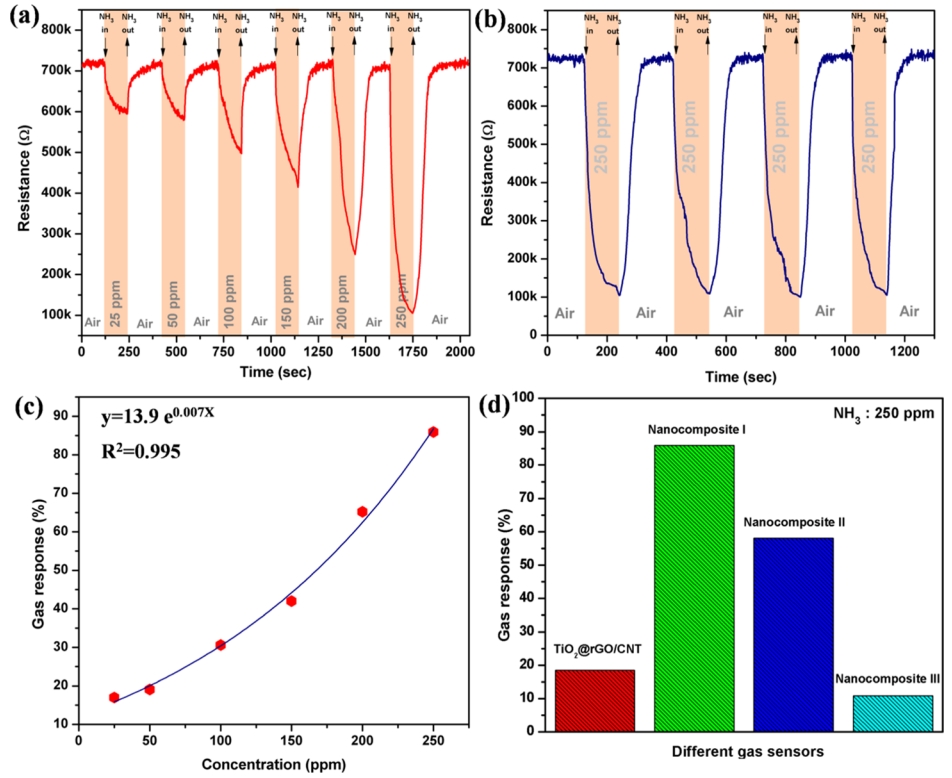

Figure 4. Changes in resistance of (a) nanocomposite I gas sensors to ammonia vapor with various concentrations and (b) four repeated pulses of 250 ppm ammonia at room temperature. (c) Gas responses of nanocomposite I gas sensor to ammonia vapor with various concentrations. (d) Gas responses of nanocomposite I to 250 ppm ammonia vapor at room temperature compared with nanocomposite II, nanocomposite III, and TiO_2@rGO/CNT gas sensors.

DOI: 10.1021/acsomega.9b02185
ACS Omega 2019, 4, 16916−16924

TiO_2@rGO/CNT gas sensor indicates its good reproducibility for NH_3 detection at room temperature. The stability of the Sn−TiO_2@rGO/CNT nanocomposite gas sensor has been investigated with exposure to 250 ppm ammonia for 30 days. Based on storage of gas sensor at room temperature with uncontrolled relative humidity (RH), a slight gas response drop (only about 3%) could be observed after 30 days (see Figure S1 in the Supporting Information). It indicates that the Sn−TiO_2@rGO/CNT nanocomposite gas sensor exhibits good stability over 30 days.

The nanocomposite I gas sensor as a function of NH_3 concentration at room temperature is shown in Figure 4c. It can be seen that the gas response increases exponentially over the NH_3 concentration range of 25−250 ppm. The gas responses of the nanocomposite I gas sensor at 25, 50, 100, 150, 200, and 250 ppm NH_3 are 17.0, 19.1, 30.6, 42.0, 65.2 and 85.9%, respectively. The gas response as functions of NH_3 concentration (C_{NH_3}) can be fitted by a power law function relation according to the equation: $S = 13.9\, e^{0.007 C_{NH_3}}$ with a good correlation coefficient (0.995). The calculated response and recovery times of the nanocomposite I gas sensor for detection of 250 ppm NH_3 are 99 and 66 s, respectively, which are relatively short for a room-temperature sensor.

The effect of different molar ratios of Sn/Ti on the gas response toward 250 ppm NH_3 vapor at room temperature was investigated as shown in Figure 4d. It can be observed that the gas response increases from 18.5 to 85.9% after adding Sn/SnO_2 to TiO_2@rGO/CNT nanocomposites. However, more Sn/SnO_2-loading contents into the TiO_2@rGO/CNT nanocomposites (nanocomposite II and nanocomposite III) exhibit a decrease in response. Thus, nanocomposite I is the optimal condition of the Sn−TiO_2@rGO/CNT gas sensor that yields the highest NH_3 response at room temperature. The observed results may be explained based on the formation of p−n heterojunctions. The gas response of the nanocomposite sensor has been improved after adding Sn/SnO_2 due to the increasing number of Sn/SnO_2 nanoparticles corresponding to the number of p−n heterojunctions on the surfaces. The increasing number of Sn/SnO_2 nanoparticles on TiO_2@rGO/CNT surfaces may enlarge the specific surface area of the sensing film to absorb more oxygen molecules on the sensing film surface and increase the interface of p−n heterojunction. When the Sn/SnO_2 loading amount becomes too high, the Sn/SnO_2 molecules may aggregate into larger nanoparticles or cover the active centers of the nanocomposite, leading to a reduced number of p−n heterojunctions, causing a lower response. To distinguish the performance contribution of each ingredient within the nanocomposites, rGO/CNT and Sn−TiO_2 gas sensors were fabricated and tested toward 250 ppm NH_3 at room temperature (see Figure S2 in the Supporting Information). One can observe that the initial resistances of the rGO/CNT and Sn−TiO_2 gas sensors are too low and too high, respectively, whereas the resistance of the Sn−TiO_2@rGO/CNT sensor is between the resistance of rGO/CNT and Sn−TiO_2 sensors. The resistance of the rGO/CNT sensor increases and Sn−TiO_2 sensor resistance decreases in the present of NH_3 according to p-type and n-type characteristics, respectively. The gas responses of the rGO/CNT sensor and Sn−TiO_2 are calculated to be 30.0 and 28.8%, respectively. These results confirm the benefit of p−n heterojunction formation that gives better gas responses than pure p-type or n-type materials, that is over 55% for sensing NH_3 at room temperature.

The selectivity of the optimal Sn−TiO_2@rGO/CNT gas sensor has been characterized toward various gases including toluene (C_7H_8), dimethylformamide (DMF), acetone (C_3H_6O), ammonia (NH_3), ethanol (C_2H_6O), methanol (CH_3OH), isopropanol (C_3H_8O), formaldehyde (CH_2O), thinner, hydrogen (H_2), carbon dioxide (CO_2), and acetylene (C_2H_2) at concentrations as shown in Figure 5. It can be seen

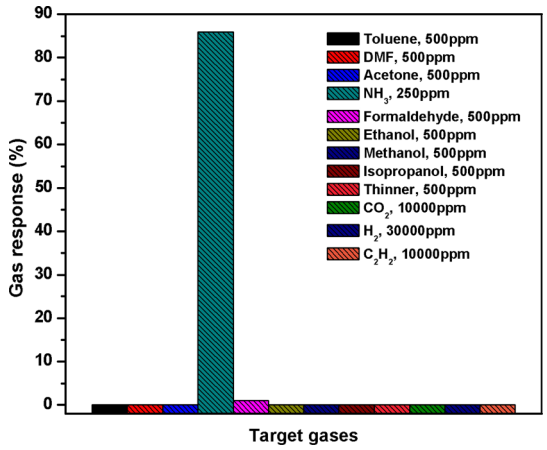

Figure 5. Selectivity histogram of the nanocomposite I gas sensor to various gases/VOCs at room temperature.

that the optimal Sn−TiO_2@rGO/CNT gas sensor exhibits ultrahigh selective NH_3 over several tested gases at room temperature. The high selectivity toward NH_3 may be related to the interaction between polarity of NH_3 molecules and hydroxyl groups on the Sn−TiO_2 surface leading to strong chemisorptions, whereas it is too difficult for other tested gases to form hydrogen bonds with these hydroxyl groups on the Sn−TiO_2 surface at room temperature.[51] Moreover, NH_3 molecules were favorable to promoting molecular adsorption on the surface acidity of Sn−TiO_2 existing Lewis acid sites (Sn^{4+} and Ti^{4+}) and Brønsted acid sites (Sn−OH and Ti−OH).[52] To investigate the humidity effect, the resistance of the Sn−TiO_2@rGO/CNT sensor was measured in real time at various humidity levels from 30 to 90% RH (see Figure S3 in the Supporting Information). It is seen that the sensor resistance does not change significantly in the range of 30−70% RH at room temperature. At high humidity level (RH > 70%), the sensor resistance decreases with increasing RH. However, when humidity response of the Sn−TiO_2@rGO/CNT sensor (defined as $[R_{30\%RH} - R_X] \times 100/R_{30\%RH}$, where $R_{30\%RH}$ and R_X are the sensor resistance values at 30% RH and the target value at another RH, respectively) is calculated, the sensor exhibits only 13.8% at 90% RH that is lower than the NH_3 gas response for all tested NH_3 concentrations (25−250 ppm). Thus, it can confirm the humidity-independent sensor for normal living condition. Moreover, the NH_3-sensing performance of the optimal Sn−TiO_2@rGO/CNT gas sensor in this study is superior to other recent reports of room-temperature NH_3 as listed in Table 1.

2.3. Sensing Mechanism of Sn−TiO_2@rGO/CNT Nanocomposite Gas Sensor. From the results, the resistance changing behaviors may be attributed to the adsorption and desorption of NH_3 molecules on the Sn−TiO_2@rGO/CNT nanocomposite sensing film. The NH_3-sensing mechanisms of

DOI: 10.1021/acsomega.9b02185
ACS Omega 2019, 4, 16916−16924

Table 1. Comparison between the Present Study and Other Reported Ammonia Gas Sensors Operating at Room Temperature

materials	response (%)	ammonia (ppm)	refs
$CuSbS_2$ QDs/rGO composites	42[a]	250	53
PANI/Fe_3O_4	47[a]	300	54
OP-G/G channel	29.3[a]	1000	55
CCO−Co(10)	7.9[a]	400	56
O_2 functional groups on rGO	3.1[a]	300	57
0.1-Pt QDs/WS_2 NSs	14.1[b]	500	58
TiO_2QDs/WS_2 nanohybrids	43.75[b]	250	59
graphite oxide	30[a]	500	60
SnO_2/rGO hybrids	4.73[a]	300	61
Sn−TiO_2@rGO/CNT	85.9[a]	250	this work

[a] $\Delta R/R_a \times 100$. [b] $\Delta I/I_a \times 100$.

the Sn−TiO_2@rGO/CNT nanocomposite gas sensor at room temperature may be explained based on the formation of p−n heterojunctions between p-type rGO/CNT and n-type metal−oxide−semiconductor (MOS) of Sn−TiO_2.[62−64] In air, oxygen species (O_2^-) chemisorbed on the surface of Sn−TiO_2@rGO/CNT nanocomposite film will capture free electrons from the conduction band of Sn−TiO_2 and the Fermi level of rGO/CNT according to the surface reaction: (1) O_2 (ads) + e^- → O_2^- (ads), leading to the formation of surface depletion layers on the interface of the Sn−TiO_2@rGO/CNT sensing film and cause the high resistance of the sensor in air as illustrated in Figure 6a.[65−67] Upon exposure to NH_3 vapor, NH_3 molecules as a reducing gas will react with oxygen species according to the reaction: (2) $4NH_3$ (gas) + $5O_2^-$ (ads) → 4NO (gas) + $6H_2O$ (gas) + $5e^-$, leading to discharge of electrons into the conduction band of Sn−TiO_2 on the sensor surface (as seen in Figure 6a).[27,68,69] This process results in a decrease of the thickness of the electron depletion layer leading to decrease in the resistance of the sensor. Moreover, the NH_3-sensing process of the Sn−TiO_2@rGO/CNT nanocomposite generates a charge between Sn−TiO_2 MOS and NH_3 molecules to electron transport through the rGO/CNT nanostructure. The rGO/CNT behaves as the electrical conduction pathway between Sn−TiO_2 grain boundaries due to the high carrier mobility of rGO/CNT. The Sn−TiO_2 nanoparticles are randomly interwoven with the rGO/CNT nanostructure to form a nanocomposite network that can enhance the surface area of the sensing film to increases the ability for adsorption and desorption of gas molecules.

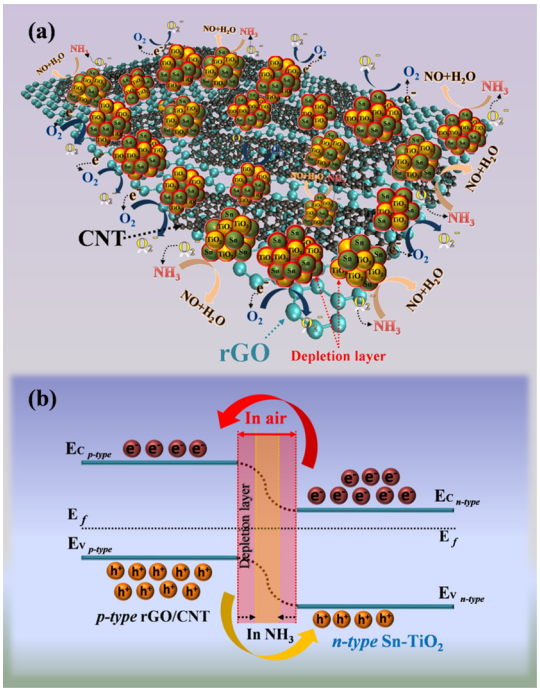

Figure 6. (a) Schematic of the proposed NH_3-sensing mechanism and (b) p−n heterojunction of the Sn−TiO_2@rGO/CNT nanocomposite gas sensor.

Furthermore, Sn−TiO_2 and rGO/CNT are typical n-type MOS and p-type semiconductors, respectively. When the p−n heterojunctions are formed, the electrons in Sn−TiO_2 will transfer to rGO/CNT, whereas the holes will transfer from rGO/CNT to Sn−TiO_2 because the n-type Sn−TiO_2 has a higher Fermi level than the p-type rGO/CNT, as shown in Figure 6b.[70−72] Once the Sn−TiO_2@rGO/CNT sensor is exposed to NH_3 vapor, the reaction between NH_3 molecules and oxygen species will occur on the n-type Sn−TiO_2 surface, so that the electrons are released from the ionized oxygen species back to the conduction band of n-type Sn−TiO_2 and combine with holes of p-type rGO/CNT, leading to reduction of the p−n heterojunction electron depletion layer width and decrease the potential barrier height ($\Delta\Phi$). The resistance of the Sn−TiO_2@rGO/CNT sensor thus decreases upon exposure to NH_3 vapor at room temperature. In addition, after the sensor is exposed to NH_3 molecules, the resistance will decrease due to the decrease of the potential barrier height at the p−n heterojunction according to the relationship: $R = B\exp(\Delta\Phi q/kT)$, where R is the sensor resistance, B is a constant, q is the electron charge, $\Delta\Phi$ is an effective the potential barrier height the p−n heterojunction, k is Boltzmann's constant, and T is the temperature of the sensing layer.[39,73]

3. CONCLUSIONS

In conclusion, Sn−TiO_2@rGO/CNT nanocomposites were successfully synthesized by the solvothermal method and systematically characterized for NH_3 sensing at room temperature. SEM, TEM, and XPS characterizations confirmed the presence of Sn−TiO_2 nanoparticles on the surface of rGO/CNT nanocomposite. As seen from the gas-sensing results, the Sn−TiO_2@rGO/CNT gas sensor demonstrated a rapid decrease of resistance upon exposure to NH_3 and fully recovered to its baseline values in air with good repeatability. The nanocomposite I gas sensor Sn−TiO_2@rGO/CNT with molar ratio of Sn/Ti (1:10) showed the highest response to NH_3 at room temperature due to balance of p−n heterojunctions and high active sensing area. Moreover, the Sn−TiO_2@rGO/CNT gas sensor exhibited ultrahigh selectivity toward NH_3 against various volatile organic compounds (VOCs) and environmental gases at room temperature with no effect of humidity in the range of 30−70% RH. The NH_3-sensing mechanism of the Sn−TiO_2@rGO/CNT nanocomposite gas sensor has been proposed based on the formation of p−n heterojunctions of p-type rGO/CNT and n-type Sn−TiO_2 via the low-temperature oxidizing reaction process. The observed ultrahigh NH_3 selectivity, high response, relatively short response, and recovery times proved that the Sn−TiO_2@rGO/CNT nanocomposite can be considered as a

DOI: 10.1021/acsomega.9b02185
ACS Omega 2019, 4, 16916−16924

promising material for practical application of NH_3 detection at room temperature.

4. EXPERIMENTAL DETAILS

4.1. Synthesis of Sn−TiO_2@rGO/CNT Nanocomposites. The synthesis process of the Sn−TiO_2@rGO/CNT nanocomposite is demonstrated in Figure 7. Graphene oxide

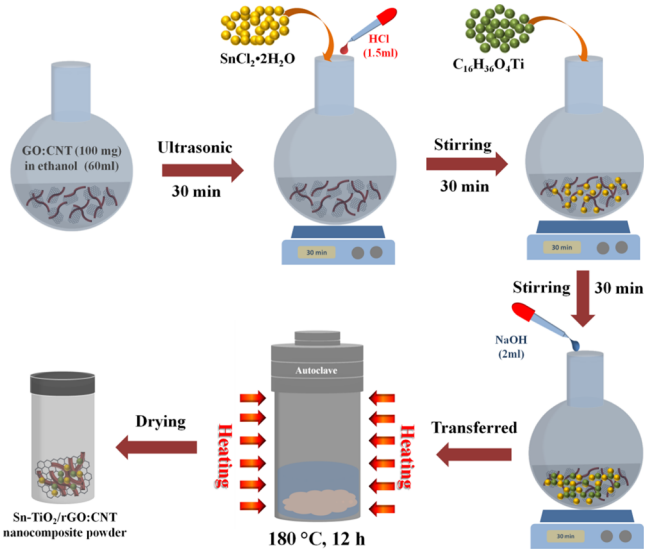

Figure 7. Schematic diagram of Sn−TiO_2@rGO/CNT nanocomposite synthesis process.

(GO) was purchased from ACS Material, LLC. CNT (with diameter 20−40 nm, length ≈ 30 μm) were purchased from Timesnano Co., Ltd. (Chengdu, China). Sn−TiO_2@rGO/CNT composites were synthesized by the solvothermal method. The amount of 100 mg of GO and CNT was dispersed in 60 mL of ethanol and treated in an ultrasonic processor for 30 min. Then, stannous chloride ($SnCl_2{\cdot}2H_2O$) and 1.5 mL of HCl (1 M) were added into the rGO/CNT solution under mechanical stirring for 30 min. Tetrabutyl titanate ($C_{16}H_{36}O_4Ti$) was mixed into the above suspension and stirred till molar ratios of Sn/Ti is 1:10. This was followed by the addition of 2 mL NaOH (1 M) dropwise and mechanically stirred for 30 min. The solution was then transferred to Teflon-lined stainless-steel autoclave and heated oven at 180 °C for 12 h. At the end of reaction, the precipitates were collected, washed with deionized (DI) water and ethanol 3 times, respectively, and then dried at 80 °C overnight to obtain the as-prepared Sn−TiO_2@rGO/CNT nanocomposites. Finally, the well crystalline solid powders were sintered at 500 °C for 3 h. In addition, the Sn−TiO_2@rGO/CNT nanocomposite with different molar ratios of Sn/Ti (3:10 and 5:10) were also produced with the same process in order to investigate the effects of Sn content on sensing properties.

4.2. Fabrication of Sn−TiO_2@rGO/CNT Nanocomposite Gas Sensors. The fabrication process of the Sn−TiO_2@rGO/CNT nanocomposite gas sensor is displayed in Figure 8. Sn−TiO_2@rGO/CNT nanocomposite powder (100 mg) was dispersed in 1 mL of DI water under ultrasonication for 5 min. The aluminum-interdigitated electrodes with the size of 4 mm × 4 mm and spacing 100 μm were prefabricated on an alumina substrate by conventional photolithography, radio-frequency sputtering, and lift-off processes. Before drop coating of the

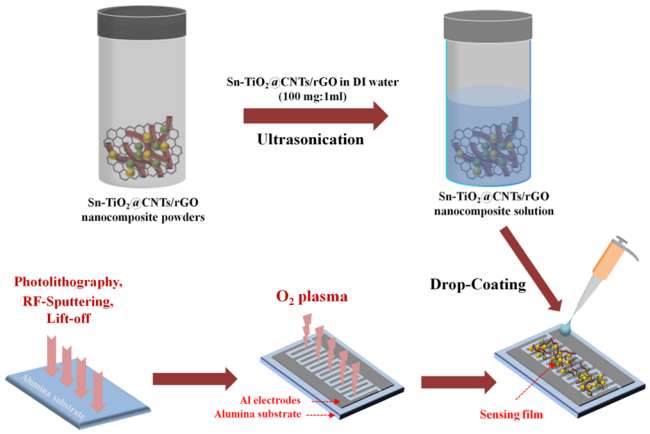

Figure 8. Schematic diagram of Sn−TiO_2@rGO/CNT nanocomposite gas sensor fabrication process.

sensing film, the aluminum interdigitated electrodes on the alumina substrate were treated by O_2 plasma in order to improve the adhesion of the sensing film on the substrates and render a hydrophilic surface. Subsequently, the Sn−TiO_2@rGO/CNT aqueous dispersion was drop-coated on the aluminum-interdigitated electrodes and dried at 80 °C. The fabricated Sn−TiO_2@rGO/CNT gas sensors with different molar ratios of Sn/Ti (1:10, 3:10, and 5:10) were defined as nanocomposite I, nanocomposite II, and nanocomposite III gas sensors, respectively.

4.3. Gas-Sensing Measurement. The gas-sensing properties of Sn−TiO_2@rGO/CNT nanocomposite gas sensors were tested in a Teflon chamber with the dynamic flow measurement. Various gases/VOCs including toluene, DMF, acetone, ammonia, formaldehyde, ethanol, methanol, isopropanol, thinner, carbon dioxide, hydrogen, and acetylene were used to evaluate the response and selectivity of fabricated gas sensors at the room temperature (26 ± 2 °C) with RH (56 ± 2%). The concentrations of test gases were varied using mass flow controllers with a flux of synthetic air. The total gas rate was fixed at 1000 sccm. The baseline of sensors was obtained by clean air for 3 min, and then the tested gas at a particular concentration was introduced into the sensor chamber for 2 min. A simple voltage divider circuit at a fixed voltage of 5 V was employed to measure the sensor resistances. The resistances of gas sensors were recorded every 1 s via a USB NI-DAQ 6008 under our developed LabVIEW software. The performances of the gas sensors were determined by means of gas response and selectivity. The gas response is defined as S (%) = $[(R_{air} - R_{gas})/R_{air}] \times 100$, where R_{air} and R_{gas} are the resistance of the fabricated gas sensor in clean air and the test gas, respectively. Selectivity is the ability of a sensor to identify a target gas that can be evaluated from relative response between different gases. The response time is defined as the time required for the sensor resistance to reach 90% of the final equilibrium signal upon exposure to the target gas, while the recovery time is the time needed to recover 90% of the initial baseline.

■ ASSOCIATED CONTENT

Supporting Information

The Supporting Information is available free of charge on the ACS Publications website at DOI: 10.1021/acsomega.9b02185.

DOI: 10.1021/acsomega.9b02185
ACS Omega 2019, 4, 16916−16924

Stability of gas sensor and changes in resistance of Sn−TiO_2 and rGO/CNT gas sensors to 250 ppm ammonia as well as the effect of humidity on sensor resistance (PDF)

AUTHOR INFORMATION

Corresponding Author

*E-mail: chatchawal.w@ku.ac.th. Phone: +662-562-5555. Fax: +662-942-8029.

ORCID

Chatchawal Wongchoosuk: 0000-0002-5613-6615

Notes

The authors declare no competing financial interest.

ACKNOWLEDGMENTS

This work was financially supported by a grant (TRF-KURDI Research Career Development Grant) from Thailand Research Fund and Kasetsart University Research and Development Institute (RSA6180062).

REFERENCES

(1) Timmer, B.; Olthuis, W.; Berg, A. v. d. Ammonia sensors and their applications-a review. *Sens. Actuators, B* **2005**, *107*, 666−677.

(2) Moos, R.; Müller, R.; Plog, C.; Knezevic, A.; Leye, H.; Irion, E.; Braun, T.; Marquardt, K.-J.; Binder, K. Selective ammonia exhaust gas sensor for automotive applications. *Sens. Actuators, B* **2002**, *83*, 181−189.

(3) Fedoruk, M. J.; Bronstein, R.; Kerger, B. D. Ammonia exposure and hazard assessment for selected household cleaning product uses. *J. Exposure Sci. Environ. Epidemiol.* **2005**, *15*, 534−544.

(4) Yang, J.; Muroyama, H.; Matsui, T.; Eguchi, K. Development of a direct ammonia-fueled molten hydroxide fuel cell. *J. Power Sources* **2014**, *245*, 277−282.

(5) Narasimhan, L. R.; Goodman, W.; Patel, C. K. N. Correlation of breath ammonia with blood urea nitrogen and creatinine during hemodialysis. *Proc. Natl. Acad. Sci. U.S.A.* **2001**, *98*, 4617−4621.

(6) Kearney, D. J.; Hubbard, T.; Putnam, D. Breath Ammonia Measurement in Helicobacter pylori Infection. *Dig. Dis. Sci.* **2002**, *47*, 2523−2530.

(7) Li, H.-Y.; Lee, C.-S.; Kim, D. H.; Lee, J.-H. Flexible Room-Temperature NH_3 Sensor for Ultrasensitive, Selective, and Humidity-Independent Gas Detection. *ACS Appl. Mater. Interfaces* **2018**, *10*, 27858−27867.

(8) Naseem, S.; King, A. J. Ammonia production in poultry houses can affect health of humans, birds, and the environment-techniques for its reduction during poultry production. *Environ. Sci. Pollut. Res.* **2018**, *25*, 15269−15293.

(9) Sankar Ganesh, R.; Navaneethan, N.; Patil, V. L.; Ponnusamy, S.; Muthamizhchelvan, C.; Kawasaki, S.; Patil, P. S.; Hayakawa, Y. Sensitivity enhancement of ammonia gas sensor based on Ag/ZnO flower and nanoellipsoids at low temperature. *Sens. Actuators, B* **2018**, *255*, 672−683.

(10) Liu, X.; Chen, N.; Han, B.; Xiao, X.; Chen, G.; Djerdj, I.; Wang, Y. Nanoparticle cluster gas sensor: Pt activated SnO_2 nanoparticles for NH_3 detection with ultrahigh sensitivity. *Nanoscale* **2015**, *7*, 14872−14880.

(11) Li, X.; Zhao, Y.; Wang, X.; Wang, J.; Gaskov, A. M.; Akbar, S. A. Reduced graphene oxide (rGO) decorated TiO_2 microspheres for selective room-temperature gas sensors. *Sens. Actuators, B* **2016**, *230*, 330−336.

(12) Mirzaei, A.; Janghorban, K.; Hashemi, B.; Bonyani, M.; Leonardi, S. G.; Neri, G. A novel gas sensor based on Ag/Fe_2O_3 core-shell nanocomposites. *Ceram. Int.* **2016**, *42*, 18974−18982.

(13) Mani, G. K.; Rayappan, J. B. B. A highly selective and wide range ammonia sensor—Nanostructured ZnO:Co thin film. *Mater. Sci. Eng., B* **2015**, *191*, 41−50.

(14) Patil, U. V.; Ramgir, N. S.; Karmakar, N.; Bhogale, A.; Debnath, A. K.; Aswal, D. K.; Gupta, S. K.; Kothari, D. C. Room temperature ammonia sensor based on copper nanoparticle intercalated polyaniline nanocomposite thin films. *Appl. Surf. Sci.* **2015**, *339*, 69−74.

(15) Detsi, E.; Cook, J. B.; Lesel, B. K.; Turner, C. L.; Liang, Y.-L.; Robbennolt, S.; Tolbert, S. H. Mesoporous $Ni_{60}Fe_{30}Mn_{10}$-alloy based metal/metal oxide composite thick films as highly active and robust oxygen evolution catalysts. *Energy Environ. Sci.* **2016**, *9*, 540−549.

(16) Shanmugam, V.; Jeyaperumal, K. S. Investigations of visible light driven Sn and Cu doped ZnO hybrid nanoparticles for photocatalytic performance and antibacterial activity. *Appl. Surf. Sci.* **2018**, *449*, 617−630.

(17) Zhou, Y.; Zou, C.; Lin, X.; Guo, Y. UV light activated NO_2 gas sensing based on Au nanoparticles decorated few-layer MoS_2 thin film at room temperature. *Appl. Phys. Lett.* **2018**, *113*, 082103.

(18) Zhou, Y.; Gao, C.; Guo, Y. UV assisted ultrasensitive trace NO_2 gas sensing based on few-layer MoS_2 nanosheet−ZnO nanowire heterojunctions at room temperature. *J. Mater. Chem. A* **2018**, *6*, 10286−10296.

(19) Xiang, C.; Chen, T.; Zhang, H.; Zou, Y.; Chu, H.; Zhang, H.; Xu, F.; Sun, L.; Tang, C. Growth of copper−benzene-1,3,5-tricarboxylate on boron nitride nanotubes and application of the composite in methane sensing. *Appl. Surf. Sci.* **2017**, *424*, 39−44.

(20) Liu, Y. Hydrothermal synthesis of TiO_2−rGO composites and their improved photocatalytic activity in visible light. *RSC Adv.* **2014**, *4*, 36040−36045.

(21) Gan, L.; Shang, S.; Yuen, C. W. M.; Jiang, S.-x.; Hu, E. Hydrothermal synthesis of magnetic $CoFe_2O_4$/graphene nanocomposites with improved photocatalytic activity. *Appl. Surf. Sci.* **2015**, *351*, 140−147.

(22) Zou, Y.; Wang, Q.; Jiang, D.; Xiang, C.; Chu, H.; Qiu, S.; Zhang, H.; Xu, F.; Sun, L.; Liu, S. Pd-doped TiO_2@polypyrrole core-shell composites as hydrogen-sensing materials. *Ceram. Int.* **2016**, *42*, 8257−8262.

(23) Zhou, Y.; Liu, G.; Zhu, X.; Guo, Y. Ultrasensitive NO_2 gas sensing based on rGO/MoS_2 nanocomposite film at low temperature. *Sens. Actuators, B* **2017**, *251*, 280−290.

(24) Wang, S.; Kang, Y.; Wang, L.; Zhang, H.; Wang, Y.; Wang, Y. Organic/inorganic hybrid sensors: A review. *Sens. Actuators, B* **2013**, *182*, 467−481.

(25) Zou, Y.; Wang, Q.; Xiang, C.; Tang, C.; Chu, H.; Qiu, S.; Yan, E.; Xu, F.; Sun, L. Doping composite of polyaniline and reduced graphene oxide with palladium nanoparticles for room-temperature hydrogen-gas sensing. *Int. J. Hydrogen Energy* **2016**, *41*, 5396−5404.

(26) Xiang, C.; Jiang, D.; Zou, Y.; Chu, H.; Qiu, S.; Zhang, H.; Xu, F.; Sun, L.; Zheng, L. Ammonia sensor based on polypyrrole−graphene nanocomposite decorated with titania nanoparticles. *Ceram. Int.* **2015**, *41*, 6432−6438.

(27) Seekaew, Y.; Lokavee, S.; Phokharatkul, D.; Wisitsoraat, A.; Kerdcharoen, T.; Wongchoosuk, C. Low-cost and flexible printed graphene−PEDOT:PSS gas sensor for ammonia detection. *Org. Electron.* **2014**, *15*, 2971−2981.

(28) Jin, G.-P.; Peng, X.; Ding, Y.-F.; Liu, W.-Q.; Ye, J.-M. Electrodeposition of platinum−nickel alloy nanocomposites on polyaniline-multiwalled carbon nanotubes for carbon monoxide redox. *J. Solid State Chem.* **2009**, *13*, 967−973.

(29) Sen, T.; Mishra, S.; Shimpi, N. G. Synthesis and sensing applications of polyaniline nanocomposites: a review. *RSC Adv.* **2016**, *6*, 42196−42222.

(30) Wisitsoraat, A.; Pakapongpan, S.; Sriprachuabwong, C.; Phokharatkul, D.; Sritongkham, P.; Lomas, T.; Tuantranont, A. Graphene−PEDOT:PSS on screen printed carbon electrode for enzymatic biosensing. *J. Electroanal. Chem.* **2013**, *704*, 208−213.

(31) Cao, F.; Zhao, M.; Yu, Y.; Chen, B.; Huang, Y.; Yang, J.; Cao, X.; Lu, Q.; Zhang, X.; Zhang, Z.; Tan, C.; Zhang, H. Synthesis of Two-Dimensional $CoS_{1.097}$/Nitrogen-Doped Carbon Nanocomposites Using Metal−Organic Framework Nanosheets as Precursors for Supercapacitor Application. *J. Am. Chem. Soc.* **2016**, *138*, 6924−6927.

DOI: 10.1021/acsomega.9b02185
ACS Omega 2019, 4, 16916−16924

(32) Stankovich, S.; Dikin, D. A.; Dommett, G. H. B.; Kohlhaas, K. M.; Zimney, E. J.; Stach, E. A.; Piner, R. D.; Nguyen, S. T.; Ruoff, R. S. Graphene-based composite materials. *Nature* **2006**, *442*, 282−286.
(33) Flahaut, E.; Peigney, A.; Laurent, C.; Marlière, C.; Chastel, F.; Rousset, A. Carbon nanotube−metal−oxide nanocomposites: microstructure, electrical conductivity and mechanical properties. *Acta Mater.* **2000**, *48*, 3803−3812.
(34) Haraguchi, K. Synthesis and properties of soft nanocomposite materials with novel organic/inorganic network structures. *Polym. J.* **2011**, *43*, 223.
(35) Li, W.; Guo, J.; Cai, L.; Qi, W.; Sun, Y.; Xu, J.-L.; Sun, M.; Zhu, H.; Xiang, L.; Xie, D.; Ren, T. UV light irradiation enhanced gas sensor selectivity of NO_2 and SO_2 using rGO functionalized with hollow SnO_2 nanofibers. *Sens. Actuators, B* **2019**, *290*, 443−452.
(36) Lim, S. P.; Pandikumar, A.; Lim, Y. S.; Huang, N. M.; Lim, H. N. In-situ electrochemically deposited polypyrrole nanoparticles incorporated reduced graphene oxide as an efficient counter electrode for platinum-free dye-sensitized solar cells. *Sci. Rep.* **2015**, *4*, 5305.
(37) Sami, S. K.; Seo, J. Y.; Hyeon, S.-E.; Shershah, M. S. A.; Yoo, P.-J.; Chung, C.-H. Enhanced capacitive deionization performance by an rGO−SnO_2 nanocomposite modified carbon felt electrode. *RSC Adv.* **2018**, *8*, 4182−4190.
(38) Wang, X.; Jia, Z.; Liu, F.; Liang, H.; You, X.; Wang, K.; Lou, X.; Shuang, W.; Xiao, L.; Cai, B.; Yang, L. The template-free synthesis of hierarchically porous anatase TiO_2 via acid-etching for enhancing the cycling stability and reversible capacity of lithium ion batteries. *RSC Adv.* **2016**, *6*, 48985−48994.
(39) Seekaew, Y.; Wisitsoraat, A.; Phokharatkul, D.; Wongchoosuk, C. Room temperature toluene gas sensor based on TiO_2 nanoparticles decorated 3D graphene-carbon nanotube nanostructures. *Sens. Actuators, B* **2019**, *279*, 69−78.
(40) Kang, Y.; Xue, Q.; Jin, P.; Jiang, J.; Zeng, J.; Chen, Y. Rhodium Nanosheets−Reduced Graphene Oxide Hybrids: A Highly Active Platinum-Alternative Electrocatalyst for the Methanol Oxidation Reaction in Alkaline Media. *ACS Sustainable Chem. Eng.* **2017**, *5*, 10156−10162.
(41) Cheong, J. Y.; Kim, C.; Jang, J. S.; Kim, I.-D. Rational design of Sn-based multicomponent anodes for high performance lithium-ion batteries: SnO_2@TiO_2@reduced graphene oxide nanotubes. *RSC Adv.* **2016**, *6*, 2920−2925.
(42) Zhang, B.; Zheng, Q. B.; Huang, Z. D.; Oh, S. W.; Kim, J. K. SnO_2−graphene−carbon nanotube mixture for anode material with improved rate capacities. *Carbon* **2011**, *49*, 4524−4534.
(43) Kumari, S.; Shekhar, A.; Pathak, D. D. Graphene oxide−TiO_2 composite: an efficient heterogeneous catalyst for the green synthesis of pyrazoles and pyridines. *New J. Chem.* **2016**, *40*, 5053−5060.
(44) Dang, M. T.; Lefebvre, J.; Wuest, J. D. Recycling Indium Tin Oxide (ITO) Electrodes Used in Thin-Film Devices with Adjacent Hole-Transport Layers of Metal Oxides. *ACS Sustainable Chem. Eng.* **2015**, *3*, 3373−3381.
(45) Gupta, A.; Dhakate, S. R.; Gurunathan, P.; Ramesha, K. High rate capability and cyclic stability of hierarchically porous Tin oxide (IV)-carbon nanofibers as anode in lithium ion batteries. *Appl. Nanosci.* **2017**, *7*, 449−462.
(46) Ni, S.; Guo, F.; Wang, D.; Jiao, S.; Wang, J.; Zhang, Y.; Wang, B.; Feng, P.; Zhao, L. Modification of TiO_2 Nanowire Arrays with Sn Doping as Photoanode for Highly Efficient Dye-Sensitized Solar Cells. *Crystals* **2019**, *9*, 113.
(47) Yao, Z.; Meng, Y.; Zhao, Y.; Liu, G.; Xia, Q.; Wang, J.; Jiang, Z. A one-step preparation and enhanced electrochemical properties of C-TiO_2 composite films. *Electrochim. Acta* **2017**, *254*, 320−327.
(48) Ahmad, Z.; Najeeb, M. A.; Shakoor, R. A.; Alashraf, A.; Al-Muhtaseb, S. A.; Soliman, A.; Nazeeruddin, M. K. Instability in $CH_3NH_3PbI_3$ perovskite solar cells due to elemental migration and chemical composition changes. *Sci. Rep.* **2017**, *7*, 15406.
(49) Khore, S. K.; Tellabati, N. V.; Apte, S. K.; Naik, S. D.; Ojha, P.; Kale, B. B.; Sonawane, R. S. Green sol−gel route for selective growth of 1D rutile N−TiO_2: a highly active photocatalyst for H_2 generation and environmental remediation under natural sunlight. *RSC Adv.* **2017**, *7*, 33029−33042.
(50) Zheng, J.; Wang, Y.; Zhang, F.; Yang, Y.; Liu, X.; Guo, K.; Wang, H.; Xu, B. Microwave-assisted hydrothermal synthesis of solid-state carbon dots with intensive emission for white light-emitting devices. *J. Mater. Chem. C* **2017**, *5*, 8105−8111.
(51) Zhou, Y.; Li, X.; Wang, Y.; Tai, H.; Guo, Y. UV Illumination-Enhanced Molecular Ammonia Detection Based On a Ternary-Reduced Graphene Oxide−Titanium Dioxide−Au Composite Film at Room Temperature. *Anal. Chem.* **2019**, *91*, 3311−3318.
(52) Li, X.; Zhao, Y.; Wang, X.; Wang, J.; Gaskov, A. M.; Akbar, S. A. Reduced graphene oxide (rGO) decorated TiO_2 microspheres for selective room-temperature gas sensors. *Sens. Actuators, B* **2016**, *230*, 330−336.
(53) Liu, Y.; Wang, H.; Chen, K.; Yang, T.; Yang, S.; Chen, W. Acidic Site-Assisted Ammonia Sensing of Novel $CuSbS_2$ Quantum Dots/Reduced Graphene Oxide Composites with an Ultralow Detection Limit at Room Temperature. *ACS Appl. Mater. Interfaces* **2019**, *11*, 9573−9582.
(54) Chabukswar, V. V.; Bora, M. A.; Adhav, P. B.; Diwate, B. B.; Salunke-Gawali, S. Ultra-fast, economical and room temperature operating ammonia sensor based on polyaniline/iron oxide hybrid nanocomposites. *Polym. Bull.* **2019**, DOI: 10.1007/s00289-019-02703-4.
(55) Wu, H.; Bu, X.; Deng, M.; Chen, G.; Zhang, G.; Li, X.; Wang, X.; Liu, W. A Gas Sensing Channel Composited with Pristine and Oxygen Plasma-Treated Graphene. *Sensors* **2019**, *19*, 625.
(56) Jain, S.; Patrike, A.; Badadhe, S. S.; Bhardwaj, M.; Ogale, S. Room-Temperature Ammonia Gas Sensing Using Mixed-Valent $CuCo_2O_4$ Nanoplatelets: Performance Enhancement through Stoichiometry Control. *ACS Omega* **2018**, *3*, 1977−1982.
(57) Minitha, C. R.; Anithaa, V. S.; Subramaniam, V.; Rajendra Kumar, R. T. Impact of Oxygen Functional Groups on Reduced Graphene Oxide-Based Sensors for Ammonia and Toluene Detection at Room Temperature. *ACS Omega* **2018**, *3*, 4105−4112.
(58) Ouyang, C.; Chen, Y.; Qin, Z.; Zeng, D.; Zhang, J.; Wang, H.; Xie, C. Two-dimensional WS_2-based nanosheets modified by Pt quantum dots for enhanced room-temperature NH_3 sensing properties. *Appl. Surf. Sci.* **2018**, *455*, 45−52.
(59) Qin, Z.; Ouyang, C.; Zhang, J.; Wan, L.; Wang, S.; Xie, C.; Zeng, D. 2D WS_2 nanosheets with TiO_2 quantum dots decoration for high-performance ammonia gas sensing at room temperature. *Sens. Actuators, B* **2017**, *253*, 1034−1042.
(60) Bannov, G. A.; Prášek, J.; Jašek, O.; Zajíčková, L. Investigation of Pristine Graphite Oxide as Room-Temperature Chemiresistive Ammonia Gas Sensing Material. *Sensors* **2017**, *17*, 320.
(61) Zhang, D.; Liu, J.; Jiang, C.; Liu, A.; Xia, B. Quantitative detection of formaldehyde and ammonia gas via metal oxide-modified graphene-based sensor array combining with neural network model. *Sens. Actuators, B* **2017**, *240*, 55−65.
(62) Wei, B.-Y.; Hsu, M.-C.; Su, P.-G.; Lin, H.-M.; Wu, R.-J.; Lai, H.-J. A novel SnO_2 gas sensor doped with carbon nanotubes operating at room temperature. *Sens. Actuators, B* **2004**, *101*, 81−89.
(63) Zhang, D.; Liu, A.; Chang, H.; Xia, B. Room-temperature high-performance acetone gas sensor based on hydrothermal synthesized SnO_2-reduced graphene oxide hybrid composite. *RSC Adv.* **2015**, *5*, 3016−3022.
(64) Li, X.; Zhao, Y.; Wang, X.; Wang, J.; Gaskov, A. M.; Akbar, S. A. Reduced graphene oxide (rGO) decorated TiO_2 microspheres for selective room-temperature gas sensors. *Sens. Actuators, B* **2016**, *230*, 330−336.
(65) Zhang, H.; Feng, J.; Fei, T.; Liu, S.; Zhang, T. SnO_2 nanoparticles-reduced graphene oxide nanocomposites for NO_2 sensing at low operating temperature. *Sens. Actuators, B* **2014**, *190*, 472−478.
(66) Seekaew, Y.; Phokharatkul, D.; Wisitsoraat, A.; Wongchoosuk, C. Highly sensitive and selective room-temperature NO_2 gas sensor based on bilayer transferred chemical vapor deposited graphene. *Appl. Surf. Sci.* **2017**, *404*, 357−363.

DOI: 10.1021/acsomega.9b02185
ACS Omega 2019, 4, 16916−16924

(67) Zhang, D.; Liu, A.; Chang, H.; Xia, B. Room-temperature high-performance acetone gas sensor based on hydrothermal synthesized SnO_2-reduced graphene oxide hybrid composite. *RSC Adv.* **2015**, *5*, 3016−3022.
(68) Zhang, D.; Jiang, C.; Sun, Y. e. Room-temperature high-performance ammonia gas sensor based on layer-by-layer self-assembled molybdenum disulfide/zinc oxide nanocomposite film. *J. Alloys Compd.* **2017**, *698*, 476−483.
(69) Ye, Z.; Tai, H.; Xie, T.; Su, Y.; Yuan, Z.; Liu, C.; Jiang, Y. A facile method to develop novel TiO_2/rGO layered film sensor for detecting ammonia at room temperature. *Mater. Lett.* **2016**, *165*, 127−130.
(70) Zhang, D.; Wu, Z.; Zong, X. Flexible and highly sensitive H_2S gas sensor based on in-situ polymerized SnO_2/rGO/PANI ternary nanocomposite with application in halitosis diagnosis. *Sens. Actuators, B* **2019**, *289*, 32−41.
(71) Kim, J.-H.; Mirzaei, A.; Kim, H. W.; Kim, S. S. Low power-consumption CO gas sensors based on Au-functionalized SnO_2-ZnO core-shell nanowires. *Sens. Actuators, B* **2018**, *267*, 597−607.
(72) Miller, D. R.; Akbar, S. A.; Morris, P. A. Nanoscale metal oxide-based heterojunctions for gas sensing: A review. *Sens. Actuators, B* **2014**, *204*, 250−272.
(73) Kim, H.-J.; Lee, J.-H. Highly sensitive and selective gas sensors using p-type oxide semiconductors: Overview. *Sens. Actuators, B* **2014**, *192*, 607−627.

DOI: 10.1021/acsomega.9b02185
ACS Omega 2019, 4, 16916−16924